Response to the TAC/iTAC Review for PR12-13-011

June 14, 2013

Executive Summary

The Jefferson Lab TAC review of PR12-13-011 noted that time-dependent instrumental drifts must be carefully monitored and suppressed. The TAC concluded that these effects can be mitigated with expected infrastructure upgrades, along with sufficient commitment from the collaboration to control these systematic effects. We examine here the impact of these contributions, and conclude that the total systematic uncertainty is of order $\mathcal{O}(10^{-3})$. This is similar in magnitude to the expected statistical uncertainty, and allows for a substantial improvement in world data.

We also discuss the promising outlook for obtaining and characterizing significant tensor polarizations in a solid target. Our initial analysis indicates that large tensor polarizations ($P_{zz} > 30\%$) with better than 12% relative systematic uncertainty can be expected.

Contents

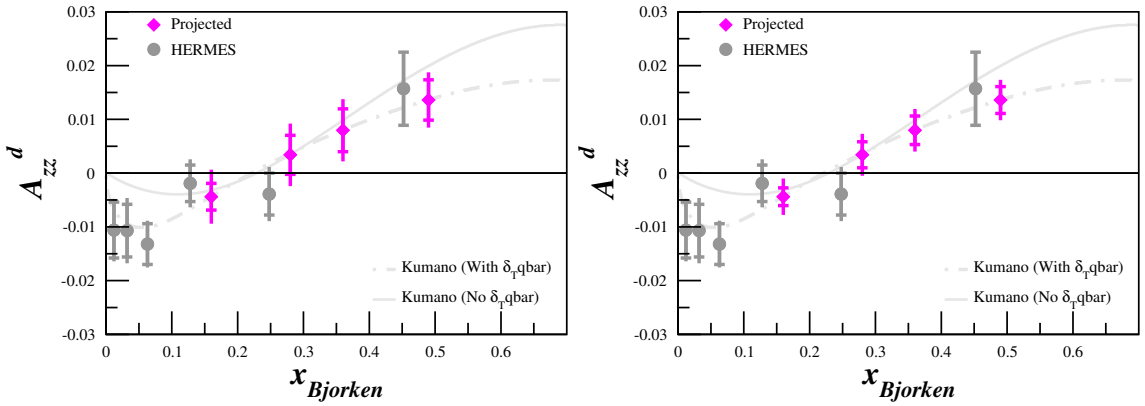

(a) Projection with $P_{zz} = 20\%$.

(b) Projection with $P_{zz} = 30\%$.

Figure 1: Projected uncertainties for A_{zz}. The inner error bars show the statistical uncertainty, while the outer bars shows systematic and statistical uncertainty combined. The Hermes error bars represent their total uncertainty. Kumano's fits to the Hermes data are also shown.

1 Overview

The TAC noted that typical instrumental drifts in Hall C can create false asymmetries of $\pm O(0.01)$, but also noted that these effects can be mitigated with a combination of upgrades to Hall C infrastructure, and sufficient commitment from our collaboration. In this document, we provide support for this conclusion by considering the instrument performance from previous experiments with similar configurations.

We note that there is a large overlap between this collaboration and the g2p (E08-027) collaboration. E08-027 similarly had a dedicated team which focused exclusively on the polarized target, but also had a separate team which focused on very demanding beamline upgrades, a team which focused on the novel optics of the septa magnet, and another which worked on the detector and DAQ performance. In this context, we believe that the current proposal's manpower requirements for systematic mitigation are not unique, and should not pose an undue burden on this collaboration.

1.1 Prospective Measurement

In general, we appreciate the TAC/iTAC's careful review of the technical aspects of this proposal, and agree with almost all of their comments. The one exception is their criticism that our measurement would be marginal since it may not discriminate between available models. This unfortunately misses the fact, that no conventional model can explain the truly unexpected large asymmetries observed by HERMES. It is also directly at odds with the Theory review (TACT) of this proposal. The TACT stated that "*With very little experimental information currently available, any new data on b1 would be clearly welcome.*" In fact, we will be able to measure these observables with considerably smaller errors than Hermes as shown in Fig. 1.

The left panel of Fig. 1 reflects the measurement previously outlined in the proposal, but explicitly shows the systematic uncertainties arising from both overall normalizing factors, and the time dependent drifts summarized in Table 1 of this document. We note that we have doubled the number of polarization cycles at the lowest x-bin in order to better match the statistical and systematic uncertainties. The normalization uncertainty has also been reduced slightly (6% relative compared to the 9% assumed in the proposal) in order to account for the smaller polarization errors enabled by the fitting technology described in Sec. A.1. The Kumano fit (which is much larger than any conventional model) to the Hermes data has been used to set the scale for determining systematic uncertainties which depends on the absolute value of A_{zz}.

The iTAC encouraged development of the target to routinely produce tensor polarization of 30% or larger, so we have evaluated the projection for this scenario as well. Tensor polarizations of 30% have been demonstrated previously [13], and as we discuss in Sec. A, the prospects for even larger tensor polarizations look very good. Increasing the polarization reduces both the statistical uncertainty and the drift systematic, as shown in Eq. 1 of this document. But the over all polarization measurement uncertainty increases, due to the complication to the NMR lineshape. We have accounted for this in the right panel by increasing the polarimetry uncertainty to 10%, which increases the overall systematic to 12%..

1.2 Drift Estimates and Mitigation

As discussed in Sec. 2.1.2 of the proposal, the time-dependent systematic drift in the observable A_{zz} is expressed as

$$\delta A^d_{zz} = \pm \frac{2}{f P_{zz}} \delta\xi, \tag{1}$$

where $\delta\xi$ contains the sum of contributions from charge (δQ), detectors ($\delta\epsilon$), target length (δl), and acceptance (δA).

The combined impact of all these systematic effects (δQ, $\delta\epsilon$, δl, δA, beam drift...) can be monitored in the measured yield. Fig. 2 shows that the unpolarized yield during the E06-010 (Transversity) experiment was stable to 0.355% over the course of 15 days running [1]. This translates to stability at the 1.1×10^{-4} level for a 12 hour cycle. One caveat is that E06-010 ran with 10 μA current, so this result will need to be verified with data from an experiment that ran at the lower currents ($\sim$ 100 nA) typical of this proposal.

1.2.1 Beam Position Drifts

At high current (50μA) the PREX (parity for lead in Hall A) experiment used regression techniques to keep the position differences [3] to about 1 nm, with angle differences less than 1 nrad. The Hall C QWeak experiment reached similar precision, which is much better than the requirements for this proposal.

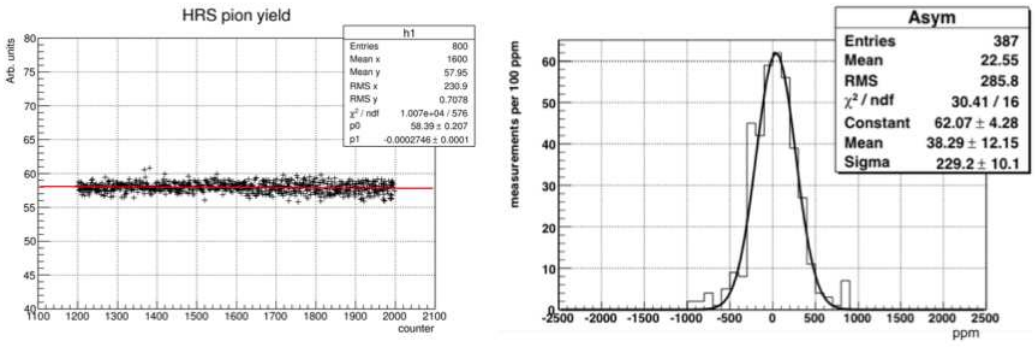

Figure 2: Data from the E06-010 (Transversity) experiment. **Left:** The measured yield drifted by 0.355% over 15 days of continuous running. This translates to stability at the 1.1×10^{-4} level for a 12 hour cycle. **Right:** The measured beam charge asymmetry over the same time was 3.8×10^{-5} with a width of 2.3×10^{-4}.

We also note that the beam will be rastered over a very large area (2 cm diameter), which dramatically reduces the impact of any small drifts in the beam position compared to an unrastered beam, even before any feedback on beam position is implemented.

1.2.2 Charge

New BCM/BPM electronics were designed for both g2p and QWeak, to reach a precision of 100 μm in position and 1% in current/charge measurement in only a few tens of milliseconds. Position resolutions of 100-200 μm and 1-2% precision in charge were verified during g2p, which allowed a slow-lock feedback system to be used.

The BCM calibration constants for the E08-027 (g2p) experiment displayed an absolute deviation of 2.0×10^{-4} over the course of six days [5].

Further minimization of long term drifts by careful thermal isolation of the BCMs, implementation of a low power (1.1 kW) Faraday Cup, and a dedicated luminosity monitor [6], were suggested by the TAC report. We will work closely with Hall C staff to implement and test these upgrades. With this in mind, we estimate deviation from unaccounted for drift for low current monitoring between the different polarization states to be no larger than the 2.0×10^{-4} observed in g2p.

1.2.3 Trigger, Cuts & Tracking Efficiency

Effects from trigger, cuts and tracking efficiency do lead to errors in normalization, however both polarization states see the same stochastic fluctuation over the course of a cycle, which leads only to a small relative uncertainty in the observable. Aspects of the error that are non-stochastic and follow an unknown trend have been estimated in the proposal in Sec. 2.1.2 under the name 'detector drifts.' Recently, we obtained a secondary estimate based on HRS detector stability using Hall A Transversity data

for detected pions as shown in Fig 2. The resulting drift was 2.2×10^{-4}, which we take as an upper limit.

In addition we intend to set detector thresholds conservatively and use meticulous on-line monitoring and checks to the relative changes in tracking efficiency between slugs.

1.2.4 Target Dilution and Length

The TAC raised the issue of possible changes to target length and dilution factor. We would like to emphasize that all changes to the material that might occur during movement of the target ladder or annealing only happen at the end of each pair of measurement cycles. Each cycle is independent and changes that happen at the end of the cycle are irrelevant for the preceding or following cycles. Historically, step-like changes in the target length or dilution are exceedingly rare and should be observable immediately from the target polarimetry which is quite sensitive to the material filling factor.

As suggested by the TAC, we will utilize a series of downstream luminosity monitors arranged symmetrically around the beam pipe, downstream of the target and in front of the Faraday cup. The lumi detectors will provide a continuous monitor of beam charge $\times$ target thickness. Discussions with the QWeak lumi experts indicate that stability at the 10^{-4} should be achievable [4] in a counting mode setup, with a slow lock on beam position and angle at the target.

The polarized material are contained in 3.0 cm long, 2.54 cm diameter cylindrical cups with their axis parallel to the beam. The cylinders fit inside the 4 cm diameter vertical cylindrical tail piece at the bottom of the refrigerator. The tail piece is full of liquid helium to about 20 cm above the beam level. The heat and radiation of the beam is distributed uniformly over the cross section of the target normal to the incident beam by a combination of slow and fast rasters. The fast raster normally is a 2mm by 2mm square shape, traced by the submillimeter beam at kHz rates. The slow raster is a 2 cm diameter spiral, traced at constant tangential speed, covering the rastered area with 5% dose uniformity at 30 Hz and can be synchronized to the usual helicity flip signals [7].

The ammonia material shape and consistency is optimized to maximize the packing fraction and minimize the fracturing capacity. It is hand selected to reduce the structural faults to obtain beads approximately 2 mm in diameter, which have already undergone multiple steps of mechanical stress including being pre-irradiated at NIST with a 10 μA beam. The UVa Target group is designing new target cups which minimize the probability of changes to target dilution from material loss. The new cups contains multiple hole arrays that are only a 0.35 mm in size. This allows for free flow of liquid helium while eliminating the possibility of material loss.

The averaging of the target length done by the rasters results in an effective length that is determined by the fraction of the cup volume within the raster that is filled with ammonia [7]. A possible change in the effective target length between the polarized and unpolarized periods of a measurement cycle could come from a net change of material in the raster volume. Since the raster diameter is 25% smaller

than the cup diameter, there is always material outside the raster region that would fill in an unlikely loss in the rastered region.

A possible estimate of the length change can be obtained by considering the ratio of the 0.008 cm^3 volume of a fragment to the 6.8 cm^3 raster volume (including packing fraction). The ratio is $\sim 1/850$.

There is only one documented instance at JLab of a possible rearrangement of material about the target NMR coil that might indicate an associated net change in material. This was seen during E07-003, SANE, which took about 500 hours of ≥ 85 nA beam, and was immediately observable as a dramatic change in the polarimetry of the sample. During one 20 h polarized and unpolarized cycle, the loss of 1 or 2 fragments would result in a $\sim 1 \times 10^{-3}$ change in target length, with a $\sim$ 20h/500h probability.

No instances of material fragmentation, which could potentially lead to net losses in the raster region have been observed with up to 150 nA CW CEBAF beams (E93-026, E01-006, E07-003). Such fragmentation would also be noticeable as a change in target polarimetry.

The temperature and thus the density of the target is kept the same in both polarized and unpolarized states. There are four temperature sensors in a standard solid polarized target setup that can be used to monitor this. The temperature is controlled via LHe evaporation, microwave, and beam heating. All three are used to maintain consistent temperature in both polarization states.

The target operating temperature is 1.1 ± 0.15 K, well below the superfluid point. For a change of 0.15 K, the LHe density, changes by 4×10^{-5} (the density actually increases below $\simeq 1.1K$ and increases above, by about equal amounts over the temperature interval [8]). The lattice constant of deuteroammonia [9] changes from 5.048 Å at 2 K to 5.073 Å at 77 K, corresponding to a 1×10^{-5} change over the ± 0.15 K interval considered above. For a 60% packing fraction the change would be 2.3×10^{-5} for a 0.15 K unexpected temperature difference between polarization states. Any possible unaccounted changes in target length between the polarized and unpolarized parts of each cycle can also be monitored by recording the time dependence of the luminosity with a $\simeq 0.5 \times 10^{-4}$ accuracy. The Hall C lumis provide this level accuracy in counting mode [4].

In summary, we consider that the contribution of the non-statistical time dependence of the target length to the measurement error will not exceed one part in 10,000 for each cycle. In the possible occurrence of target bead shifts the effect is easily averaged out in the rastered volume to be negligible as is the loss of a bead during a single polarization cycle.

1.2.5 Depolarizing the Target

We stress that we are able to depolarize the target with a mixture of destructive microwave pumping and using Adiabatic Fast Passage via the NMR rf coil. It is not necessary to drain liquid helium to depolarize, although this is the most efficient method.

x	Hours	Stat. Error (10^{-3})	Cycles	Drift Error (10^{-3})
0.15	144	2.6	12	4.3
0.30	216	3.0	9	4.9
0.45	360	3.7	15	3.8
0.55	720	4.1	36	2.4

Table 1: The estimated drift of the A_{zz} asymmetry measurement.

1.2.6 Solid Angle

The error that arises in the observable due to beam position and magnet currents over time is inherently very difficult to separate into drift and relative uncertainty. The 0.1% error over a 12 hour period suggested by the TAC is probably accurate. However, we note that both polarization states experience the same fluctuations, such that the majority of the uncertainty is relative. There are also concerns on acceptance due to beam position drift. Beam drift can be monitored during the experiment and accounted for during analysis. We consider the largest part of this uncertainty to also be a relative contribution to both target states. The contribution to the drift can be minimized with the feedback system built for parity experiments (regression).

Trends that arise from dependence of yield on magnet currents in detectors are a concern related to the spectrometer acceptance. The drift effect can be made to be small, for HRS typically less than 10^{-4} for the dipole and 10^{-3} for the three quads. We assume similarly for HMS. The effects on the acceptance can be determined and corrected through careful analysis. Naturally the target magnet current does not need to be changed between cycles, the uniformity, stability, and setability pointed out in the proposal eliminate field variation between the two polarization states. We expect a residual drift from solid angle effects after such correction to be no larger than 0.01%. This value was already accounted for in Section 1.2.3.

1.2.7 Final Drift Estimate Per Point

Using the values presented here for each component that can contribute to the drift we obtain a value no larger than 4.0×10^{-4} in $\delta\xi$ of Eq. 1. We see this as an over estimate of what we can achieved using the out-lined mitigation techniques. This estimate is based on previous data prior to the the upgrades to the Hall C infrastructure, so naturally we expect to do better.

To determine the actual drift in observable δA_{zz}^d (false asymmetry) over the course of the experiment we look at the number of measurements (cycles) at each point. Since the times at each point are different, the number of cycles is not the same for all points. There are only three independent points, since the HMS data is collected in parallel. For the $x = 0.15$, we have doubled the number of cycles in order to minimize the drift for that point. For the other points, the need for statistics outweighs the need to reduce the drift. Table 1 shows the resulting drift in the asymmetry for each independent kinematic point in x. The time for each cycle for $x = 0.15$ are actually half as long so the value of δA_{zz}^d would ultimately be significantly smaller than the

estimate in the table.

1.3 Other Systematic Effects

1.3.1 Beam Polarization

The beam helicity information can be used to count buckets equally in the two helicity states, so the use of incident polarized beam does not present a challenge to our experiment. The parity beam feedback system typically reduces the charge asymmetry between the two states to the 50 ppm level. As an example, the E06-010 (Transversity) experiment [1] used 80% polarized beam (with appropriate averaging) to extract the single spin asymmetry from a polarized target. The beam charge asymmetries between two helicity states using the luminosity monitors was shown to be at the level of 3.8×10^{-5} with a width of 2.3×10^{-4}, as shown in Fig. 2. Similar results 9.6×10^{-5} with a width of 1.5×10^{-4} were found [2] in the g2p experiment, which ran at typical currents of 50-100 nA.

1.3.2 Parity Violating Asymmetries

The TAC raised the question of how parity violating asymmetries may impact our measurement. The relevant asymmetry A_{EW} is expected to be about 4×10^{-4} [14] for $Q^2 < 5$ GeV^2. We further discussed this issue with Wally Melnitchouk, who noted that the PV contribution is very small and can be calculated in terms of spin-dependent PDFs, so in the DIS region the uncertainty from this would be expected to be small. These small effects will be further suppressed by flipping the direction of the target vector polarization at the end of each unpolarized/polarized cycle.

A Improving Tensor Polarization and Polarimetry Uncertainty

The UVA target group has been able to produce 50% vector polarization with the trend in polarization still increasing. This is with the standard UVA pump system at the university. The UVA pump system now at Jefferson Lab has much greater cooling power. We expect to be able to achieve a tensor polarization much greater than the 12% mentioned by the TAC, even without hole-burning. In addition developments are underway that can be used to measure the tensor polarization after hole-burning. The lack of measuring capacity and large polarization uncertainty has been the biggest block for employing the hole-burning technique. The development and implementation of the technique has broad implication for experiments to come, but will require the dedicated effort of a PhD student, or post-doctoral researcher.

A.1 Line Shape Fitting

The SMC group has developed an analytic model [10] of the deuteron absorption function used to determine the deuteron vector polarization. The absorption func-

tion model includes dipolar broadening and a frequency-dependent treatment of the intensity factors. The TE signal data can be used to adjust the model for Q-meter distortions and dispersion effects. Once the Q-meter adjustment is made, the enhanced polarizations determined by the SMC fitting and TE-calibration methods agree very well within the accuracy of each method.

The spin system can be irradiated by radio frequency (RF) energy and if that irradiation occurs at the Larmor frequency the spins either absorb or emit some energy. The response of a spin system to RF irradiation is described by its magnetic susceptibility which leads to a direct relation of the ensemble spin system population of states and the area of the signal voltage as a function of the real part of the magnetic susceptibility and RF frequency ω. The polarization for the deuteron can be expressed as,

$$P = C \int \frac{\omega_d S(\omega)}{\omega} d\omega. \tag{2}$$

Here, C is a constant representing the frequency-independent gains in the Q-meter, $S(\omega)$ is the NMR signal for the deuteron absorption function whose maximum occurs at its Larmor frequency ω_d. The signal only extends over about a $2\pi \times 300$ kHz range, outside of which the dispersion function can be considered to have constant value. This relationship indicates that the total integrated area of the NMR signal is directly proportional to the material polarization.

The SMC model incorporates first-order quadrupole splitting with electric field gradients. The symmetry configuration of the deuteron and corresponding bonds leads to local electric field gradients that couple to the quadrupole moments of the deuteron causing an asymmetric splitting of the energy levels into two overlapping absorption lines. The two peaks (See Fig. 13 of the proposal) seen in the shape of absorption lines reflect the net number of spins available for making a particular transition.

For a given value of the angle between the axis given by the deuteron bond and the magnetic field there are two resonant frequencies in this system which correspond to the positive $E_0 \Leftrightarrow E_1$ transition with energy $\Delta E_+ = E_0 - E_1$ and intensity I_+ and the negative $E_{-1} \Leftrightarrow E_0$ transition with energy $\Delta E_- = E_{-1} - E_0$ and intensity I_-.

A fit function based on this model which uses the dipolar broadening of the density of states with a Lorentzian convolution was also developed by the SMC group. The result is a fit function to obtain the intensities $I_\pm$ of the two overlapping absorption peaks. The relation $r = I_+/I_- = n_+/n_-$ assumes a Boltzmann distribution among the sub-levels so that the vector polarization can be expressed as

$$P = (r^2 - 1)/(r^2 + r + 1), \tag{3}$$

and the tensor polarization can be expressed as,

$$P_{zz} = (r^2 - 2r + 1)/(r^2 + r + 1). \tag{4}$$

For vector polarization above 30% the line shape fitting technique can be made accurate to 3% relative. The great advantage here is that the error in area and calibration constant from the TE-calibration are completely side stepped. The majority of error

from the fitting technique is fitting error and background subtraction. This is especially useful for determining the tensor polarization as compared to using the analytic relation $P_{zz} = 2 - \sqrt{4 - 3P^2}$ for which the tensor polarization error propagates to roughly double the vector polarization error.

Dramatic improvements in the NMR signal to noise ratio has been demonstrated recently [12] using the so-called 'cold NMR' technique, which moves much of the traditional Q-meter circuit onto the target insert near the pickup coil. This technique was recently verified at Jefferson Lab, and has also been implemented at UVa.

Using the line shape fitting combined with the cold NMR technique, it is within reason to expect to be able to cut our polarization uncertainty listed in the proposal by 50%. The cold NMR reduces systematic effects over time significantly. In addition the UVA target group is presently devolving a fitting algorithm based on the SMC peak asymmetry fitting technique.

A.2 Optimizing Polarization Through RF-saturation

The technique of manipulating the fraction of the spins in the magnetic sub-levels with a saturating RF field can be done in such a way as to optimize the resulting tensor polarization. The optimization is done by irradiating the sample with a frequency-modulated RF field around the peak and pedestal position for either the $E_{-1} \Leftrightarrow E_0$ or $E_0 \Leftrightarrow E_1$ transitions. RF saturation takes about 10 minutes leaving the m=0 and either the m=1 or m=−1 with approximately the same populations. The only new components are an additional RF coil and amplifier. The coil design will need to ensure maximal material RF saturation, while minimizing any impact on the experimental acceptance, but otherwise there are no new specialized hardware requirements.

The population of the m=0 level will have been increased relative to the Boltzmann population level leading the tensor polarization to increase to the same degree. For complete saturation, the initial vector polarization and resulting tensor polarization will be equal in magnitude. Neglecting any spin-spin relaxation during the procedure, this would imply tensor polarizations of 40-45% are very plausible. Even without complete saturation, it has been demonstrated that the tensor polarization can be roughly doubled as compared to what is achievable with microwaves alone [11]. These results need verification and further study but are very promising to our objective.

Improvement to the expected polarization, although not strictly necessary, would allow the addition of kinematic points, improved statistical accuracy and the reduction of the error contribution from drift δA^d_{zz}. The reduction to this error is seen analytically in Eq. 1. The value of δA^d_{zz} is reduce by the same factor that the polarization is increased.

A.3 Measuring the RF-saturation Signal

It is important to measure the dynamic NMR signal for all possible line shapes and spin state populations through the experiment. This can be done by using an extension to the line shape fitting technique which relates the area of the fitted absorption

lines to the population of states. Through the course of the hole burning RF modulation, the dipolar broadening of the density of states is altered in a calculable way. For example, an area translation from the m=0 $\rightarrow$ m=1 transition to enhance tensor polarization can be measured by comparing the fitted area from the SMC method prior to hole burning RF modulation with a Riemann sum of the reduced region. The ratio, r_0, of the remaining non-translated area to the initial area gives the fractional increase from the available enhancement to the tensor polarization. The increase to the tensor polarization relative to the Boltzmann population level can then be added to the previously measured initial tensor polarization (prior to RF modulation). The hole burning tensor polarization can be expressed as,

$$P_{zz}^{HB} \approx \frac{A^{NMR}}{A^I} \left(P_{zz}^I + r_0 (P^I - P_{zz}^I) \right). \tag{5}$$

Here P^I and P_{zz}^I come from the fit to the signal after the area has been maximized but prior to RF modulation, A^{NMR} is the signal area and A^I is the signal area that was maximized prior to RF modulation. The values for P^I and P_{zz}^I come from Eq. 3 and 4 respectively and so the error from these terms is not large. The largest error in r_0 would be primarily from the uncertainty in Riemann sum for the remaining non-translated area. For small areas this is around 2%. There could be larger error for scenarios where the hole had not yet burned through to cleanly separate the two peaks so that a clean boundary for the Riemann sum can be established. Including the fit and area errors total error would be about 5-7% relative. This method is just a first step and is not well established but it does give a way to estimate the polarization using the hole burning technique at various degrees of saturation. A more encompassing model and fit function will be developed in the near future. From a conservative stand point we expect to be able to achieve less than 10% relative uncertainty in the tensor polarization after hole burning.

References

[1] Kalyan Allada, Hall A Staff. Personal communication, 2013.

[2] Melissa Cummings, College of William and Mary. Personal communication, 2013.

[3] Mark Dalton, PREX Collaboration. Jefferson Lab User Group Meeting, May 2013. `http://www.jlab.org/conferences/ugm/talks/thur/MarkDalton_UserGroup_NeutronRadius.pdf`

[4] Mark Pitt, QWeak Collaboration. Virginia Tech. Personal Communication, 2013.

[5] Pengia Zhu, University of Science and Technology of China (USTC). Personal communication, 2013.

[6] Dave Mack, Hall C staff. Personal communication, 2013.

[7] Chen Yan, JLab HAll C Technical Note, http://hallcweb.jlab.org/document/howtos/slow_raster.pdf

[8] Russell J. Donelly, http://pages.uoregon.edu/rjd/vapor2.htm

[9] A. W. Hewat and C. Riekel, *Acta Cryst.* (1979) A **35**, 569

[10] C. Dulya, et al. Nucl. Instr. and Meth. in Phys. Res. A 398, 109 (1997)

[11] W. Meyer and E. Schilling, BONN-HE-85-06, C84-09-03.1 (1985)

[12] G.R. Court, et al. Nucl. Instr. and Meth. in Phys. Res. A 527, 253 (2004)

[13] Results of Research Run 11/30/99-2/11/00, S. Bueltmann, D. Crabb, and Y. Prok UVA-Tech-Note (2000).

[14] P. Anthony et al., E155x collaboration, *Phys. Lett.* **B**553, 18 (2003).